Int. J. Heat Mass Transfer. Vol. 26, No. 3, pp. 451 458, 1983
Printed in Great Britain

0017-9310/83/030451-08 $03.00/0
Pergamon Press Ltd.

THREE-DIMENSIONAL NATURAL CONVECTION IN A CONFINED POROUS MEDIUM WITH INTERNAL HEAT GENERATION

K. J. BEUKEMA* and S. BRUIN†

Department of Process Engineering, Agricultural University Wageningen, De Dreijen 12, 6703 BC Wageningen, The Netherlands

and

J. SCHENK

Department of Physics, Agricultural University Wageningen, Duivendaal 1, 6701 AP Wageningen, The Netherlands

(*Received* 30 *November* 1981)

Abstract—A model of three-dimensional natural convection in a confined porous medium with internal heat generation was developed. The governing equations were reduced to one parabolic and one elliptic differential equation. Experiments were performed on cooling model material, representing agricultural products, at different rates of heat generation (0–235 Wm^{-3}) in a closed container (0.76 m × 0.76 m × 0.50 m) with isothermal walls. Compared with conduction only, natural convection accelerated cooling, gave a lower average temperature and moved the location of the maximum temperature from the centre of the container upwards. Measured and calculated cooling curves could be brought into good agreement by introduction of a wall heat transfer coefficient in the model equations.

NOMENCLATURE

c_p,	heat capacity at constant pressure [$Jkg^{-1}K^{-1}$];
g,	acceleration of gravity [ms^{-2}];
$\mathbf{O}$,	vorticity vector [s^{-1}];
P,	pressure [Pa];
Q,	rate of heat generation [Wm^{-3}];
R_1, R_2, R_3,	container dimensions [m];
t,	time [s];
T,	temperature [°C];
T_0,	outside temperature [°C];
T_s,	initial temperature [°C];
$\mathbf{v}$,	velocity [ms^{-1}];
V,	velocity potential [m^3s^{-1}];
x, y, z,	distance coordinates [m].

Greek symbols

α,	heat transfer coefficient [$Wm^{-2}K^{-1}$];
β,	thermal expansion coefficient [K^{-1}];
θ,	dimensionless temperature, $(T-T_0)/(T_s-T_0)$;
θ_Q,	dimensionless temperature, $(T-T_0)\lambda/QR_3^2$;
κ,	permeability [m^2];
λ,	bulk thermal conductivity [$Wm^{-1}K^{-1}$];
ρ,	density [kgm^{-3}];
μ,	dynamic viscosity [$kgm^{-1}s^{-1}$];
ψ,	vector potential [m^2s^{-1}].

Subscripts

a,	air;
m,	medium;
r,	reference value;
sw,	side wall.

Superscript

$\bar{}$,	average value.

INTRODUCTION

NATURAL convection in porous media with internal heat generation is of interest in such situations as post accident heat removal in nuclear power reactors and the geophysical problems arising during the storage of nuclear waste in the earth [1, 2]. We are interested in quite another field where this kind of natural convection occurs, namely during the storage of agricultural products. Agricultural products are stored to be available over longer periods. During storage, agricultural products generate heat as a result of metabolism of the products. Storage at about 0°C normally gives the longest optimal storage time. Thus, when harvested products go into store it is usually necessary to cool them down to about 0°C.

When cooling air is blown around a container with products, whereas the container wall is impervious to air flow, heat is transported by conduction in the container to the wall (conductive cooling). As a consequence of the resulting temperature differences in the container, natural convection occurs. The air flow in the container is directed downwards at the wall and upwards in the central part of the container. When

* Present address: AVEBE Research, Kl. Nieboerweg 12, 9607 PN Foxhol, The Netherlands.
† Present address: Unilever Research Laboratories, Olivier van Noortlaan 120, 3133 AT Vlaardingen, The Netherlands.

cooling air is blown through a container with products or bulk stored products (convective cooling), natural convection occurs too. We have discussed this elsewhere [3].

In the calculation of cooling rates and temperature distributions in closed containers [4, 5] for the purpose of the design of cold storage facilities, the influence of natural convection is always neglected. However, natural convection will occur. Therefore this study aims to investigate the influence of natural convection on cooling rates and temperature distributions during the storage of agricultural products in closed containers.

As with convective cooling [3], the products in the container are considered to behave as a porous medium. Several studies on natural convection in porous media with internal heat generation have been performed. The literature deals with the onset of natural convection [1, 6, 7], the acceleration of heat transfer [8, 9] and the stability of different kinds of fluid flow [7, 10]. However all authors describe horizontally infinite layers, whereas we are interested in natural convection in a confined porous medium. A confined porous medium has been discussed in the description of natural convection caused by a temperature difference between top and bottom [11–14].

We have analysed natural convection in a rectangular porous medium with internal heat generation theoretically, starting from the work of Holst and Aziz [11] and Tveitereid [7]. The validity of the model developed is tested by comparing measured and calculated temperatures during the cooling of a model material.

MODEL EQUATIONS

In the derivation of the model equations the general equations for continuity, momentum and energy are simplified by neglecting inertia forces in the momentum equation and viscous heating by fluid flow in the energy equation. The Boussinesq approximation is applied. The Darcy term is used to represent the viscous term in the momentum equation. Heat generation is assumed to be uniformly distributed in the porous medium. The energy equation is derived for a one-phase model.

With these assumptions the governing equations are

Continuity equation.

$$\nabla \cdot \mathbf{v} = 0. \tag{1}$$

Equation of motion.

$$\rho_r \frac{\partial \mathbf{v}}{\partial t} = -\nabla P + \rho_r[1 - \beta(T - T_r)]\mathbf{g} - (\mu/\kappa)\mathbf{v}. \tag{2}$$

Energy equation.

$$(\rho c_p)_m \frac{\partial T}{\partial t} + (\rho c_p)_a \mathbf{v} \cdot \nabla T = \lambda \nabla^2 T + Q. \tag{3}$$

Aziz and Hellums [15] showed that in a fluid-filled parallelepiped the elimination of pressure in the equation of motion leads to a set of equations which are solved more easily than the original set of equations. Holst and Aziz [16] showed that this elimination may also be applied for a porous medium. Pressure is eliminated by the vector potential–vorticity method. Vector potential ($\boldsymbol{\psi}$) and vorticity ($\mathbf{O}$) are defined by

$$\mathbf{v} = \nabla \times \boldsymbol{\psi}, \tag{4}$$

$$\mathbf{O} = \nabla \times \mathbf{v}. \tag{5}$$

The vector potential may be looked upon as the 3-dim. extension of the 2-dim. stream function. Hirasaki and Hellums [16] showed that, when $\mathbf{v}$ is solenoidal ($\nabla \cdot \mathbf{v} = 0$), $\boldsymbol{\psi}$ exists and is solenoidal. The equation of continuity shows that $\mathbf{v}$ is solenoidal and therefore $\boldsymbol{\psi}$ is solenoidal. This property of the vector potential combined with the definition of the vorticity leads to

$$\mathbf{O} = \nabla \times \mathbf{v} = \nabla \times (\nabla \times \boldsymbol{\psi}) = -\nabla^2 \boldsymbol{\psi}. \tag{6}$$

Analysis of equations (2) and (3) showed that velocity attained the steady state much faster than temperature. Therefore, being interested in the temperature course, the time derivative of $\mathbf{v}$ may be neglected in equation (2). This yields

$$\mathbf{v} = -\frac{\kappa}{\mu}\{\nabla P - \rho_r[1 - \beta(T - T_r)]\mathbf{g}\}. \tag{7}$$

Because $\nabla \times \nabla P = 0$, the vorticity is

$$\mathbf{O} = \frac{\kappa}{\mu}\nabla \times (\rho_r[1 - \beta(T - T_r)]\mathbf{g}) = -\frac{\kappa}{\mu}\nabla \times (\rho_r \beta T \mathbf{g}). \tag{8}$$

Combination of equations (6) and (8) with $\mathbf{g} = (0, 0, g)$ yields

$$\nabla^2 \psi_x = -\frac{\kappa}{\mu}\frac{\partial}{\partial y}(\rho_r g \beta T), \tag{9}$$

$$\nabla^2 \psi_y = \frac{\kappa}{\mu}\frac{\partial}{\partial x}(\rho_r g \beta T), \tag{10}$$

$$\nabla^2 \psi_z = 0. \tag{11}$$

The boundary conditions of this set of equations are given by the system: a rectangular parallelepiped with the walls which are impervious to fluid flow (Fig. 1).

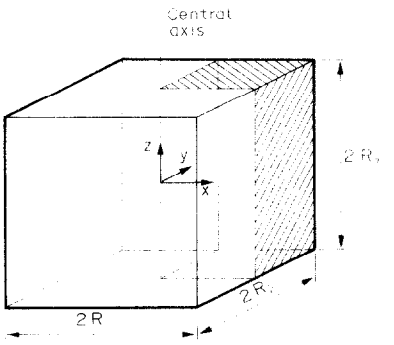

FIG. 1. The rectangular parallelepiped.

Because of the symmetry in the parallelepiped the governing equations need only to be solved in a quarter of the parallelepiped. The quarter of interest is indicated in Fig. 1. The centre of the coordinate system is located in the centre of the parallelepiped. The bottom, right side, back and top are rigid and therefore the fluid velocity is zero at these walls. At the left side and front, fluid flow is possible.

Hirasaki and Hellums [16] derived the boundary conditions of the vector potential on the walls without fluid flow,

$$x = R_1, \quad \frac{\partial \psi_x}{\partial x} = \psi_y = \psi_z = 0, \tag{12}$$

$$y = R_2, \quad \psi_x = \frac{\partial \psi_y}{\partial y} = \psi_z = 0, \tag{13}$$

$$z = -R_3, R_3, \quad \psi_x = \psi_y = \frac{\partial \psi_z}{\partial z} = 0. \tag{14}$$

Equation (11) with boundary condition (14) gives

$$\psi_z = 0. \tag{15}$$

The boundary conditions of ψ_x and ψ_y are completed with the symmetry conditions

$$x = 0, \quad \frac{\partial \psi_x}{\partial x} = 0, \quad \psi_y = 0, \tag{16}$$

$$y = 0, \quad \psi_x = 0, \quad \frac{\partial \psi_y}{\partial y} = 0 \tag{17}$$

The initial condition of ψ is

$$t = 0, \quad \psi_x = \psi_y = 0. \tag{18}$$

Of course, initial and boundary conditions for the temperature are required too. We assumed symmetry around the x, z-plane and y, z-plane and described heat transfer at the walls with a constant overall heat transfer coefficient. In the overall heat transfer coefficient both the influence of inside and outside wall heat transfer coefficient and of heat conduction through the wall are summarized. The initial temperature distribution is assumed to be uniform. This yelds

$$t = 0, \forall (x, y, z), \quad T = T_s, \tag{19}$$

$$t > 0, \forall (y, z), \quad x = 0, \quad \frac{\partial T}{\partial x} = 0, \tag{20}$$

$$\forall (y, z), \quad x = R_1, \quad -\lambda \frac{\partial T}{\partial x} = \alpha_{sw}(T - T_0), \tag{21}$$

$$\forall (x, z), \quad y = 0, \quad \frac{\partial T}{\partial y} = 0, \tag{22}$$

$$\forall (x, z), \quad y = R_2, \quad -\lambda \frac{\partial T}{\partial y} = \alpha_{sw}(T - T_0), \tag{23}$$

$$\forall (x, y), \quad z = R_3, \quad -\lambda \frac{\partial T}{\partial z} = \alpha_t(T - T_0), \tag{24}$$

$$\forall (x, y), \quad z = -R_3, \quad \lambda \frac{\partial T}{\partial z} = \alpha_b(T - T_0). \tag{25}$$

By solving the coupled differential equations (3), (9) and (10) with appropriate boundary conditions, the temperature and velocity at different times and different locations in the container may be calculated. However this set of equations contains two elliptic differential equations of which the numerical solution is very computer-time consuming. Tveitereid [7, 17] introduced the velocity potential (V), which reduced the two elliptic differential equations to one. He defined the velocity potential only in terms of velocity

$$v_x = \frac{\partial^2 V}{\partial x \partial z}, \tag{26}$$

$$v_y = \frac{\partial^2 V}{\partial y \partial z}, \tag{27}$$

$$v_z = -\left(\frac{\partial^2 V}{\partial x^2} + \frac{\partial^2 V}{\partial y^2}\right). \tag{28}$$

There exist, of course, relations between velocity potential and vector potential

$$\psi_x = \frac{\partial V}{\partial y}, \tag{29}$$

$$\psi_y = -\frac{\partial V}{\partial x}. \tag{30}$$

With these relations equations (9) and (10) may be reduced to

$$\nabla^2 V = -\frac{\rho_r g \beta \kappa}{\mu}(T - T_r). \tag{31}$$

The boundary conditions of V are derived from those of ψ

$$t = 0, \quad \forall (x, y, z), \quad V = 0, \tag{32}$$

$$t > 0, \quad \forall (y, z), \quad x = 0, R_1, \quad \frac{\partial V}{\partial x} = 0, \tag{33}$$

$$\forall (x, z), \quad y = 0, R_2, \quad \frac{\partial V}{\partial y} = 0, \tag{34}$$

$$\forall (x, y), \quad z = -R_3, R_3, \quad V = 0. \tag{35}$$

The equations (3) and (31) are both solved with an Alternative Direction Implicit Procedure [18]. Further details are given elsewhere [19].

To calculate the driving force of natural convection in the container the reference air density (ρ_r) should be calculated from the average temperature in the container (T_r). We used

$$\rho_r = \frac{353.15}{(273.13 + T_r)}. \tag{36}$$

EXPERIMENTAL

The geometrical and climatological conditions in our experiments are based on those occurring during the storage of agricultural products. We used a brass container (0.76 m × 0.76 m × 0.50 m) with isothermal walls, filled with a model material. The wall

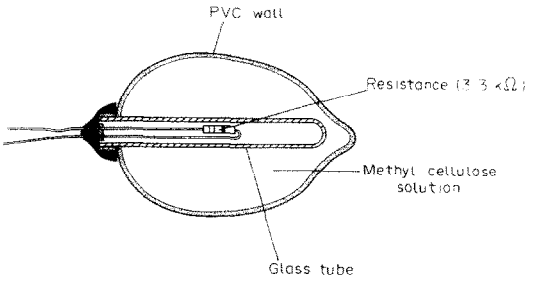

FIG. 2. Construction of the model material, developed at the Sprenger Institute, Wageningen.

temperature was kept constant by pumping methanol from a thermostatic bath through pipes which had good thermal contact with the six walls of the container. The model material (Fig. 2), which was developed at the Sprenger Institute, Wageningen, has a heat capacity and dimensions which are about the same as those of real agricultural products. Heat generation occurred by applying a voltage to the resistor in the centre of the model material. The temperature at different locations in the container was measured with thermistors, using an automatic measuring system. With this system 75 different temperatures could be measured. Further details are given elsewhere [19]. The top of the container could be removed to fill the container. Five holes, which were closed during the experiments, were made in the bottom to enable air to be blown through the container for cooling or heating by forced convection.

The experimental procedure started with heating the model material up to about 30°C by forced convection. After closing the container, wall cooling and a selected rate of heat generation by the model material were started. At the start of an experiment, temperatures at different locations in the container did not differ by more than 1.0°C. At the start temperatures were measured every 30 min. The period between two measurements was gradually increased up to about 6 h at the end of an experiment. An experiment was stopped after about 180 h when the steady state was attained. By these measurements information was obtained on temperature development during transient cooling and on steady state temperature distribution at different rates of heat generation.

RESULTS AND DISCUSSION

The measured temperature course at different positions along the central axis of the container at a rate of heat generation of 60 Wm^{-3} is shown in Fig. 3. The wall temperature in this experiment was 19.2°C. The temperature course at 0.150 and 0.195 m is most remarkable. About 10 h after the start of the experiment, a decreasing rate of cooling which afterwards changed to heating was observed. This is caused by the influence of heat transport by natural convection. Just after the start of an experiment,

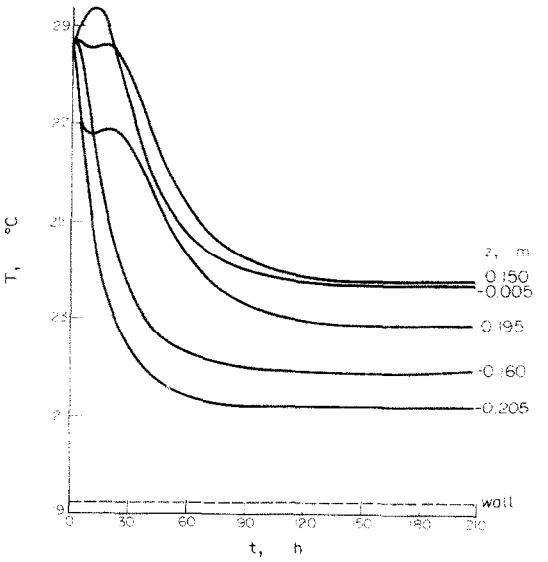

FIG. 3. Measured changes in temperature with time along the central axis with $Q = 60$ Wm^{-3} and $T_0 = 19.2$°C.

temperature differences in the container are only small and therefore the velocity of natural convection is small too. The cooling rate of the container at that very moment is determined by heat conduction, giving fast cooling near the wall and heating in other parts of the container. After cooling for about 10 h, temperature differences in the container become larger. As a result the velocity of natural convection increases and convective heat transport in the container becomes more important. The air flows downwards near the cold walls and upwards in the central part of the container. The rising air causes heat transport from the lower to the upper part of the container. This explains the remarkable temperature course at 0.150 and 0.195 m. In all experiments a slower decrease or faster increase of temperature with time after cooling about 10 h is observed at $z = 0.150$ m (Fig. 4), even without heat generation. It appears from Fig. 4 that it depends upon the rate of heat generation whether cooling or heating occurs at $z = 0.150$ m at beginning of an experiment.

Figure 5 gives the steady state temperature distribution along the central axis at different rates of heat generation. In this figure the temperature is given as the dimensionless temperature θ_Q

$$\theta_Q = \frac{(T - T_0)\lambda}{QR_3^2}. \tag{37}$$

When using θ_Q the temperature profiles for conductive cooling only, with isothermal walls, are equivalent at different rates of heat generation. This theoretical temperature profile of conductive cooling only is also indicated in Fig. 5. The figure shows also, that at one height the dimensionless steady-state temperature decreases with increasing rate of heat generation. With increasing rate of heat generation the actual maximum temperature differences in the container increase. The

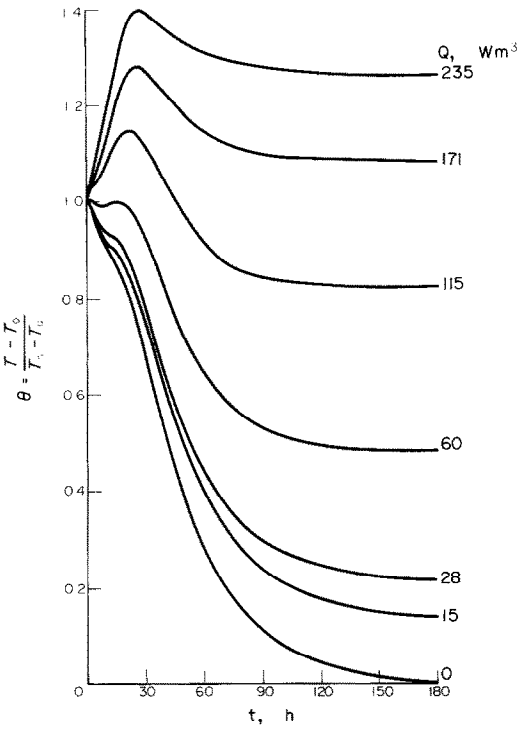

FIG. 4. Measured changes in temperature with time at $x = 0$, $y = 0$ and $z = 0.150$ m with different rates of heat generation.

resulting higher velocity of natural convection causes more effective heat transport and thus more heat loss to environment. One can imagine that this results in a value of θ_Q that will be smaller when the rate of heat generation increases.

Under conditions where conduction is the only mechanism of heat transport the maximum temperature is located in the centre of the container. Figure 5 shows a rise in position of the maximum temperature at increasing rate of heat generation. As the air flows upwards in the central part of the container, the rise in

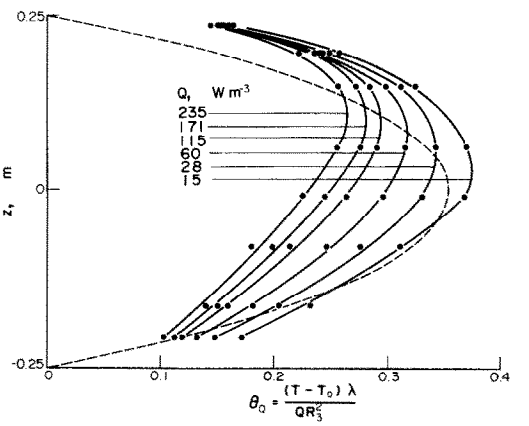

FIG. 5. Measured steady state profile of dimensionless temperature along the central axis with different rates of heat generation. ——— Pure conduction, $\lambda = 0.25$ Wm^{-1}K^{-1}.

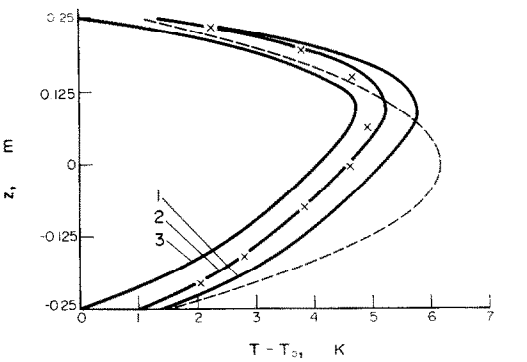

FIG. 6. Calculated distribution of steady-state temperature along the central axis for different heat transfer coefficients at the walls. (1) $\alpha_b = 5$ Wm^{-2}K^{-1}, $\alpha_t = 9$ Wm^{-2}K^{-1} and $\alpha_{sw} = 6.5$ Wm^{-2}K^{-1}. (2) $\alpha_b = 7$ Wm^{-2}K^{-1}, $\alpha_t = 10$ Wm^{-2}K^{-1} and $\alpha_{sw} = 20$ Wm^{-2}K^{-1}. (3) $\alpha_b = 1000$ Wm^{-2}K^{-1}, $\alpha_t = 1000$ Wm^{-2}K^{-1} and $\alpha_{sw} = 1000$ Wm^{-2}K^{-1}. x Measured temperatures. ——— Profile for conduction only and values of set (2).

position is caused by the higher velocity of natural convection at increasing rate of heat generation.

Figure 5 further reveals a resistance to heat transfer near the isothermal wall. This resistance may be modelled with a wall heat transfer coefficient, well known from the theories of catalytic fixed bed reactors [20, 21]. It is possible to estimate the value of this wall heat transfer coefficient from an extrapolation of the measured temperature profile to the wall. In our experiments this method is rather inaccurate because only a few temperatures are measured near the wall. The wall heat transfer coefficient may also be estimated by comparing measured temperature profiles with temperature profiles calculated with the model equations (3) and (31). Figures 6 and 7 show the

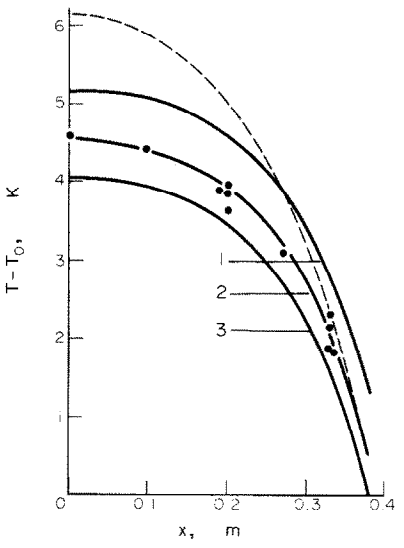

FIG. 7. Calculated distribution of steady-state temperature in the x direction ($y = 0$ and $z = 0$) for different heat transfer coefficients at the wall. Legend: see Fig. 6. ● = Measured in positive and negative x and y direction.

measured and calculated steady state temperature profile in the z- and y-direction, respectively, at $Q = 60$ Wm^{-3} and different heat transfer coefficients at the wall. The value of the physical properties used in the calculations are given in Table 1. The figures show that temperature profiles of correct shape are obtained by using the following set of wall heat transfer coefficients at bottom (α_b), top (α_t) and side walls (α_{sw}): $\alpha_b = 7$, $\alpha_t = 10$ and $\alpha_{sw} = 20$ $Wm^{-2}K^{-1}$. The calculated temperature profile for conductive cooling only with the heat transfer coefficients given above is also given in Figs. 6 and 7. The influence of natural convection is obvious.

In our calculations symmetry around the x, z- and y, z-planes was assumed. In order to check the assumed symmetry, the temperature was measured at different symmetrical positions. Figure 7 gives the measured temperatures in positive and negative x- and y-directions at a distance of 0.20 and 0.33 m from the central axis. The small scatter in temperature proves that the assumed symmetry in the container is reasonable. Temperature measurements at other symmetrical positions gave comparable results.

Apart from predicting the steady-state temperature distribution, the model equations are also derived to calculate the temperature course during the cooling period. Figure 8 shows that the course of the measured temperatures is predicted very well by the model calculations. Measured and calculated values of θ never differ more than 4%. For the sake of clearness only some of the measured temperatures are shown in Fig. 8.

The calculated change of average temperature with time at cooling with and without natural convection is shown in Fig. 9. Both curves are calculated with the model equations, the data of Table 1 and the wall heat transfer coefficients given above. In case of cooling without natural convection, only the energy balance with $\mathbf{v} = 0$ had to be solved. Figure 9 shows that after an initial period of about 10 h where the influence of natural convection is still negligible, cooling with natural convection proceeds faster. With natural convection the calculated average temperature in the steady state is 11% lower than when natural convection is neglected. The influence of natural convection increases when the rate of heat generation is higher.

In order to compare the results on model material

Table 1. Data used in the calculations

Rate of heat generation (Q)	60 Wm^{-3}
R_1	0.38 m
R_2	0.38 m
R_3	0.25 m
Initial temperature (T_s)	28.75°C
Outside temperature (T_0)	19.2°C
Permeability (κ)	1.45×10^{-6} m^2
Bulk thermal conductivity (λ)	0.25 $Wm^{-1}K^{-1}$
Heat capacity air $[(\rho c_p)_a]$	1230 $Jm^{-3}K^{-1}$
Heat capacity medium $[(\rho c_p)_m]$	2.30×10^6 $Jm^{-3}K^{-1}$
Dynamic viscosity (μ)	1.77×10^{-5} $kgm^{-1}s^{-1}$

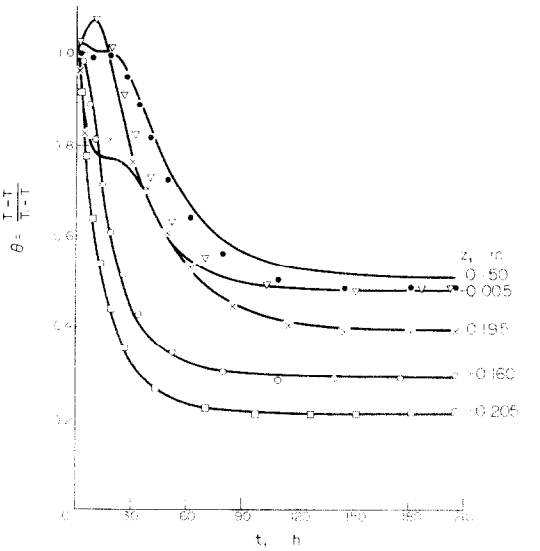

FIG. 8. Measured and calculated(———) temperature changes with time at different locations along the central axis. $Q = 60$ $Wm^{-2}K^{-1}$, $\alpha_b = 7$ $Wm^{-2}K^{-1}$, $\alpha_t = 10$ $Wm^{-2}K^{-1}$ and $\alpha_{sw} = 20$ $Wm^{-2}K^{-1}$.

with cooling of real products, some experiments were performed while the container was filled with potatoes or Brussels sprouts. With these products also, a rise of the location of the maximum temperature from the centre of the container was observed. A difference between real products and our model material is the occurrence of moisture loss in the case of real products. This causes moisture condensation in the container. The influence of moisture loss has to be incorporated in the model equations. However the solution of the resulting set of equations will require much more computer time than the solution of the actual model. Therefore we have not yet performed these calculations.

In this study we have shown that the model of 3-dim. natural convection in a confined porous medium with internal heat generation is able to predict the

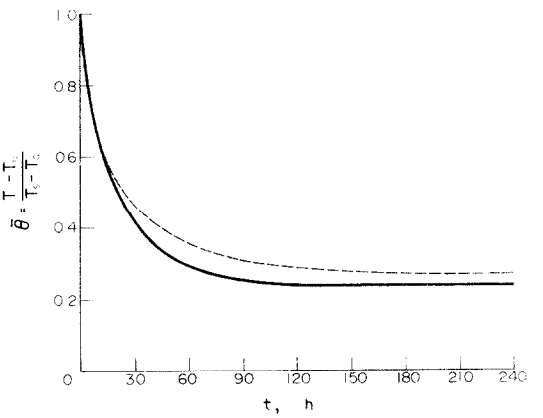

FIG. 9. Calculated changes in average container temperature with time, $Q = 60$ Wm^{-3}. – – – Without natural convection. ——— With natural convection.

temperature course in a rectangular container with heat generating model material. At the walls of the container a resistance to heat transport occurs which is modelled with an overall heat transfer coefficient. When natural convection occurs, the average and the maximum temperature in the steady state are lower than without natural convection. Because the storage of agricultural products at a lower temperature allows a longer storage period, natural convection is favourable. The results of this study obviously show that conductive cooling models are not sufficient to describe the temperature history of agricultural products which are stored in a container. The influence of natural convection may not be neglected in design of cold storage facilities.

REFERENCES

1. F. A. Kulacki and R. Ramchandani, Hydrodynamic instability in a porous layer saturated with a heat generating fluid, *Wärme und Stoffübertragung* **8,** 179–185 (1975).
2. H. C. Hardee and R. H. Nilson, Natural convection in porous media with heat generation, *Nucl. Sci. Engng* **63,** 119–132 (1977).
3. K. J. Beukema, S. Bruin and J. Schenk, Heat and mass transfer during cooling and storage of agricultural products, *Chem. Engng Sci.* **37,** 291–298 (1982).
4. H. F. Th. Meffert and M. L. Potters, Development of the temperature field in a cube with heat generation, *Ann. Bull. IIR* 1970–1, 97–106 (1970).
5. J. Eelkman Rooda and F. P. H. van Beckum, Heat-transfer during the cooling process of exponential heat generating produce, *Lebensm. Wiss. Technol.* **2,** 209–214 (1978).
6. R. D. Gasser and M. S. Kazimi, Onset of convection in a porous medium with internal heat generation, *J. Heat Transfer* **98,** 49–54 (1976).
7. M. Tveitereid, Thermal convection in a horizontal porous layer with internal heat sources. *Int. J. Heat Mass Transfer* **20,** 1045–1050 (1977).
8. R. J. Buretta and A. S. Berman, Convective heat transfer in a liquid saturated porous layer, *J. appl. Mech.* **43,** 249–253 (1976).
9. W. J. Sun, Convective instability in superposed porous and free layers, Ph.D. Thesis, Univ. of Minnesota (1973).
10. A. Zebib and D. R. Kassoy, Three dimensional natural convection motion in a confined porous medium, *Physics Fluids* **21,** 1–3 (1978).
11. P. H. Holst and K. Aziz, Transient three-dimensional natural convection in confined porous media, *Int. J. Heat Mass Transfer* **15,** 73–90 (1972).
12. J. L. Beck, Convection in a box of porous material saturated with fluid, *Physics Fluids* **15,** 1377–1383 (1972).
13. A. Zebib and D. R. Kassoy, Onset of natural convection in a box of water saturated porous media with large temperature variation, *Physics Fluids* **20,** 4–9 (1977).
14. J. M. Strauss and G. Schubert, On the existence of three-dimensional convection in a rectangular box containing fluid-saturated porous material, *J. Fluid Mech.* **87,** 385–394 (1978).
15. K. Aziz and J. D. Hellums, Numerical solution of the three-dimensional equations of motion for laminar natural convection, *Physics Fluids* **10,** 314–324 (1967).
16. G. J. Hirasaki and J. D. Hellums, A general formulation of the boundary conditions on the vector potential in three-dimensional hydrodynamics, *Q. appl. Math.* **26,** 331–342 (1968).
17. M. Tveitereid, Thermal convection in a horizontal fluid layer with internal heat sources, *Int. J. Heat Mass Transfer* **21,** 335–339 (1978).
18. J. Douglas Jr. and H. H. Rachford Jr., On the numerical solution of heat conduction problems in two and three space variables, *Trans. am. math. Soc.* **82,** 421–439 (1956).
19. K. J. Beukema, Heat and mass transfer during cooling and storage of agricultural products as influenced by natural convection, Thesis Agric. Univ. Wageningen (1980); Agric. Res. Rep. 897, Pudoc, Wageningen (1980).
20. J. J. Lerou and G. F. Froment, Velocity, temperature and conversion profiles in fixed bed catalytic reactors, *Chem. Engng Sci.* **32,** 853–861 (1977).
21. C. H. Li and B. A. Finlayson, Heat transfer in packed beds—a reevaluation, *Chem. Engng Sci.* **32,** 1055–1066 (1977).

CONVECTION NATURELLE TRIDIMENSIONNELLE DANS UN MILIEU POREUX CONFINE AVEC GENERATION INTERNE DE CHALEUR

Résumé—On développe un modèle de convection naturelle tridimensionnelle dans un milieu poreux confiné, avec génération interne de chaleur. Les équations de base sont réduites à une équation différentielle parabolique et une elliptique. Des expériences sont faites sur un matériau d'épreuve, rêsentant des produits agricoles, à différents niveaux de génération de chaleur (0–235 W m^{-3}) dans un réservoir clos (0,76 m × 0,76 m × 0,50 m) avec des parois isothermes. Comparée à la conduction seule, la convection naturelle de refroidissement accéléré donne une température moyenne plus basse et déplace le point de température maximale du centre vers le haut du conteneur. Des courbes de refroidissement mesurées et calculées peuvent être amenées à un bon accord en introduisant un coefficient de transfert thermique en paroi dans les équations du modèle.

DREIDIMENSIONALE FREIE KONVEKTION IN EINEM EINGESCHLOSSENEN PORÖSEN MEDIUM MIT INNEREN WÄRMEQUELLEN

Zusammenfassung—Es wurde ein Modell für die Berechnung der dreidimensionalen freien Konvektion in einem eingeschlossenen porösen Medium mit inneren Wärmequellen entwickelt. Die Systemgleichungen wurden auf eine parabolische und eine elliptische Differentialgleichung reduziert. Es wurden Experimente zur Kühlung von Modell-Material, das landwirtschaftliche Produkte darstellen soll, bei unterschiedlichen Intensitäten der inneren Wärmeerzeugung (0–250 W m^{-3}) in einem geschlossenen Behälter (0,76 m × 0,76 m × 0,50 m) mit isothermen Wänden durchgeführt. Verglichen mit reiner Wärmeleitung ergab die durch freie Konvektion beschleunigte Kühlung eine niedrigere mittlere Temperatur und verschob die Lage des Temperaturmaximums vom Mittelpunkt des Behälters nach oben. Gemessene und berechnete Abkühlungskurven konnten in gute Übereinstimmung gebracht werden, indem man einen Wärmeübergangskoeffizienten zur Behälterwand in das Rechenmodell einführte.

ТРЕХМЕРНАЯ ЕСТЕСТВЕННАЯ КОНВЕКЦИЯ В ЗАМКНУТОЙ ПОРИСТОЙ СРЕДЕ С ВНУТРЕННИМ ИСТОЧНИКОМ ТЕПЛА

Аннотация — Разработана модель трехмерной естественной конвекции в замкнутой пористой среде с внутренним источником тепла. Определяющие уравнения сведены к одному параболическому и одному эллиптическому дифференциальным уравнениям. Эксперименты проводились с образцами тепловыделяющих материалов, представляющих собой сельскохозяйственные продукты, помещенных в замкнутый контейнер размером 0,76 м $\times$ 0,76 м $\times$ 0,50 м с изотермическими стенками. Скорость выделения тепла изменялась в диапазоне от 0 до 235 Вт/м^3. По сравнению с передачей тепла только теплопроводностью естественная конвекция способствует более быстрому охлаждению, приводит к более низкому значению средней температуры и вызывает смещение положения максимума температуры вверх от центра контейнера. За счет введения в модельные уравнения коэффициента теплоотдачи от стенки можно получить хорошее совпадение между измеренными и рассчитанными кривыми охлаждения.